Effect of steam treatment time on the length and structure of single-walled and double-walled carbon nanotubes

Magdalena Kierkowicz,[a] Elzbieta Pach,[b] Ana Santidrián,[c] Ester Tobías-Rossell,[d] Martin Kalbáč,*[c] Belén Ballesteros*[b] and Gerard Tobias*[a]

[a] M.Kierkowicz, Dr. G. Tobias
Institut de Ciència de Materials de Barcelona (ICMAB-CSIC)
Campus UAB, Bellaterra, 08193 Barcelona, Spain
E-mail: gerard.tobias@icmab.es
[b] E. Pach, Dr. B. Ballesteros
Catalan Institute of Nanoscience and Nanotechnology (ICN2), CSIC and The Barcelona Institute of Science and Technology
Campus UAB, Bellaterra, 08193 Barcelona, Spain
E-mail: belen.ballesteros@icn.cat
[c] A. Santidrián, Dr. M. Kalbáč
J. Heyrovsky Institute of the Physical Chemistry
Dolejskova 3, 182 23 Prague 8, Czech Republic
E-mail: martin.kalbac@jh-inst.cas.cz
[d] E. Tobias-Rossell
Escola Universitària de Ciències de la Salut de Manresa, Universitat de Vic-Universitat Central de Catalunya
Av. Universitària 4-6, 08242 Manresa, Barcelona, Spain

Abstract: A major challenge to turn the potential of carbon nanotubes (CNTs) into customer applications is to reduce or eliminate their toxicity. Taking into account health and safety concerns intensified research efforts are conducted to improve biocompatibility of CNTs, including the development of new shortening and purification strategies. Ideally, the methods used for improving the biocomapatibility of CNTs should not alter the electronic properties of CNTs. Here, we report on the shortening of a sample containing single-walled and double-walled CNTs using steam and get new insights in the properties of the steam treated CNTs. The present study shows that short CNTs (median length ca. 200 nm) can be obtained under the reported conditions. Raman analysis reveals that wider and outer nanotubes undergo more significant changes than the narrower and inner ones, especially after a prolonged steam treatment.

Introduction

Carbon nanotubes (CNTs) have found a broad range of applications due to the combination of fascinating chemical and physical properties. These include their implementation in memory devices, energy storage, electronic systems, composite materials, catalysis and biomedical applications.[1] Early reports on toxicity of CNT samples have hindered the practical use of these nanomaterials in some areas.[2] The toxicity associated to samples of CNTs arises, in most cases, from the presence of long CNTs and from residual catalytic nanoparticles employed for the synthesis of the CNTs,[3] which in turn can dominate the properties of the material.[4] Numerous studies have shown that shortening strategies and purification of the samples from side-products improve their biocompatibility.[3b, 5] The length of as-produced CNTs is typically on the order of micrometers. There are many strategies that allow shortening of the CNTs, such as oxidative chemical treatments,[6] mechanical grinding,[7] lithography,[8] sonication[9] and electron beam cutting.[10] Among them, the most commonly employed approach consists on the use of strong acids, namely HNO_3, H_2SO_4 and their mixtures.[11] The use of such aggressive treatments leads to the disruption of the tubular structure of the CNTs, thus modifying their intrinsic properties. Therefore efforts have been devoted to control the oxidation process while preserving optical/

electronic properties of the material.[12] Furthermore, the presence of structural defects hinders the use of the inner cavities of CNTs to host selected payloads, and area that is getting an increased attention.[13] Steam being a mild oxidizing agent allows the purification and end-opening of carbon nanotubes whilst avoiding the formation of structural defects.[14] Early studies showed that once the ends are opened prolonged steam treatment results on the shortening of the nanotubes.[14b] We have recently established the length distribution of samples of multi-walled carbon nanotubes (MWCNTs) steam treated for different periods of time[15] but to date such information is not available for their single-walled and double-walled carbon nanotube counterparts (SWCNTs; DWCNTs).

Raman scattering allows following the changes in physical and chemical properties of CNTs. It is one of the most suitable techniques for studying the fundamental properties of CNTs, since it is a non-destructive, contactless, quick technique with relatively simple or no preparation required.[16] The Raman spectra of CNTs present several features, among which the most intense ones can be found in three spectral regions. First, the radial breathing mode (RBM), whose Raman shift (from 100 to 300 cm^{-1}) inversely depends on the CNTs diameter.[17] Second, the tangential mode (G-band) centered at 1588 cm^{-1}, containing an axial and a circumferential component, which can be used to distinguish between metallic and semiconducting CNTs by its line shape. And third, the second-order Raman mode is the G'-band (also known as the 2D-band), centered at around 2650 cm^{-1}.[18] Additionally, for samples containing structural defects, the disorder induced mode (D-band) is observed at around 1350 cm^{-1}. The D-band is a second-order Raman mode and is used to analyze the quality of the CNTs as it is sensitive to structural defects in the graphitic sp^2 network, like those induced by carbonaceous impurities.[16a] Moreover, in order to study electronic structure and the physical properties of CNTs doping experiments can be performed. To induce doping, electrons or holes are introduced into the electronic structure of the CNTs either by chemical reactions (introducing donors[19] or acceptors[19b, 20]), or by electrochemical charging.[21] The level of doping can be easily adjusted by applying potential. Electrochemical charging works as a double layer capacitor where the CNTs act as working electrode and the charge carriers are injected into the CNTs, while the electrolyte ions compensate the charge. In that way, extra electrons or holes are inserted in the CNTs causing changes in the electronic structure that can be followed by Raman spectroscopy. When the potential is changing, the charge transfer leads to a shift of the Fermi level, which can result in bleaching of the Raman modes in the CNTs spectra. When the van Hove singularities are filled, the associated optical transitions become blocked.[22] Therefore, Raman spectroelectrochemistry allows investigation of the changes in the physical properties of CNTs during charge transfer.

On the other hand, when it comes to length distribution analysis of CNTs, microscopy techniques take the lead. Although atomic force microscopy (AFM)[23] and transmission electron microscopy (TEM)[24], [25] have been mostly employed to assess the CNTs' length distribution, the use of scanning electron microscopy (SEM) presents substantial advantages.[5c, 26] SEM is in general more accessible than AFM and TEM and provides accurate measurements for wide areas of the sample in an easy and fast manner. Moreover most SEM samples require minimal preparation. A major problem when dealing with CNTs, especially with SWCNTs and DWCNTs, is that these nanoscopic materials tend to aggregate into bundles due to π-π interactions. Several approaches are nowadays available to debundle, at least partially, the nanotubes including the use of specific solvents[27] or by surface modification via both covalent and non-covalent approaches,[28] but the complete individualization of the nanotubes, desired for the determination of the length distribution remains a challenge. Towards this end we have developed a protocol to obtain individual CNTs spread on a support that allows the quantitative SEM determination of the length distribution of the steam shortened CNTs.

In the present work we get new insights on the role that the steam treatment plays in both length distribution and electronic structure of carbon nanotubes. A detailed Raman analyses with three laser excitation energies indicates that wider and outer nanotubes undergo more significant changes in the RBM bands than the narrower and inner ones, especially after a prolonged steam treatment.

Results and Discussion

As-received CNTs, which contain a mixture of both SWCNTs and DWCNTs (according to supplier), were steam treated at 900 ºC for different periods of time (4 h, 10 h, 15 h and 25 h), followed by an HCl wash. The yellow color that developed in the acid solution indicated the dissolution of iron nanoparticles (catalyst). The temperature was kept constant during the steam process since this parameter has already been previously investigated and optimized.[14a, 29] Both, as-received and

steam treated CNTs were dispersed in ortho-dichlorobenzene and characterized by SEM to determine the length of individual nanotubes. CNT bundles and individual nanotubes can be easily distinguished in this imaging modality (SI, Figure S1). HRTEM analysis confirmed that the individual CNTs present on the support had few nanometers in diameter, as those measured from SEM images (SI, Figure S2). Statistical analysis was performed with a sample size of 300 for each of the groups, namely control group (as-received) and treated groups (steam + HCl). The resulting histograms are presented in Figure 1. Visual inspection of the SEM images and the histograms already reveals that the length of the as-received CNTs decreases after exposing the material to steam. The length distribution of each of the studied groups does not follow a normal distribution, so it is not correct to determine an average mean value with the associated standard deviation to reflect the length distribution of each group. It is therefore necessary to perform a non-parametric analysis of the data. Figure 2 shows the box plot analysis of both as-received and the steam treated CNTs, and Table 1 contains the descriptive analysis. We employed non-parametric tests to assess whether the median and the length distribution of two given groups had significant differences or not. The median test was used for the former, and both the U test of Mann- Whitney and the Kolmogorov-Smirnov test, for independent groups, were employed for the latter. The null hypotheses (H_0) were respectively: "medians are the same" and "length distributions are the same". Analyses of the as-received and 4 h steam treated CNTs resulted in $p < 0.05$ for all the performed tests thus rejecting H_0. This implies that the medians and the length distribution of the CNTs are significantly different. A 40 % decrease of the median value is observed between the as-received ($median_{as\text{-}received}$ = 711 nm) and the 4 h steam treated CNTs ($median_{4h}$ = 420 nm). CNTs treated for 4 h and 10 h with steam also present significant differences ($p < 0.05$), with ca. 50% decrease of the median length between both groups ($median_{10h}$ = 198 nm). Interestingly, longer exposure of the CNTs to the steam treatment does not significantly alter the median and the length distribution of the resulting material. The statistical hypothesis testing of the CNTs treated with steam for 10 h and 15 h show no significant differences (p-value > 0.05), and the same occurs when testing the 15 h and 25 h groups. Therefore, steam is an efficient shortening method that allows the preparation of CNTs with median lengths of ca. 200 nm after 10 h treatment. After this period of time, no significant changes are observed in the length distribution of the CNTs up to 25 h steam treatment. Whereas more than 25 % of CNTs were longer than 2 µm in the as-received material, after 10-25 h of steam treatment ca. 50 % nanotubes are shorter than 200 nm and 80 % are below 500 nm. It is worth noting that the statistical analysis has been performed with large sample populations (N = 300 per group) thus leading to reliable conclusions.

Next Raman spectroscopy and in situ Raman spectroelectrochemistry with 3 different excitation energies (1.96 eV (633 nm), 2.33 eV (532 nm) and 2.54 eV (488 nm) were performed to understand the influence of steam on the physical and structural properties of the CNTs. Initially, the as-received CNTs were analyzed by in situ Raman spectroelectrochemistry in order to obtain more detailed information about its electronic structure. The potential-dependent Raman spectra (excited at 1.96 eV) of the as-received CNTs in acetonitrile electrolyte solution are shown in Figure 3, for the whole spectral range. Figure 3a, b, c and d show the RBM mode, the D-band, the G-band and the G'-band regions, respectively. When applying positive potentials, from 0 V to +1.5 V, in steps of 0.3 V, the Fermi level is downshifted (p-doping, introducing holes into the π-band). The opposite occurs when negative potentials are applied, from 0 V to -1.5 V, the electron density increases due to the upshift in the Fermi level (n-doping, introducing electrons into the π-band).[22b] In this way, when the Fermi level reaches the van Hove singularity level, the corresponding electronic transition is blocked and the Raman signal is bleached. The Raman spectrum at 0 V after applying the potential recovers its original shape, indicating that electrochemical doping of the as-received CNTs is a reversible process.

As can be seen in Figure 3, the decrease of the spectral intensity is more evident in the case of the RBM bands than in the case of the G-band. Using the RBM frequency, the theoretical diameter of the nanotubes (d_t) can be estimated according to Equation 1: $\omega = 217/d_t + 15$.[17] Only the CNT species whose transition energies (denoted as E_{ii}) are in resonance with (or close to) the energy of the laser show RBM bands in the Raman spectrum. According to the Kataura plot, the energy of the band gap in a CNT (E_{ii}) is related to its diameter.[30] Figure 3a is divided into three regions: orange, yellow and grey, each range of the RBM modes correspond to tubes excited via the electronic transitions of CNTs so-called E_{33}^S, E_{11}^M and E_{22}^S, respectively for the 1.96 eV laser energy

used. Hence, both semiconducting and metallic CNTs of the as-received CNTs are in resonance with the 1.96 eV laser energy.

The peaks at around 200 cm^{-1} (d_t= 1 nm), 215 cm^{-1} (d_t= 0.94 nm), and 221 cm^{-1} (d_t= 0.92 nm), represent metallic nanotubes, while the peaks at 156 cm^{-1} (d_t= 1.27 nm) and at 259 cm^{-1} (d_t= 0.79 nm), correspond to semiconducting nanotubes.

The G-band appears at 1588 cm^{-1} (Figure 3c.). The position of the G-band is upshifted for high anodic potentials in contrast to high cathodic potentials, in which the G-band position remains nearly constant. At high potential values, the G-band splits into 2 modes, this is an indication of the presence of double-walled carbon nanotubes (DWCNTs).[31] In this way, the G^--contribution, at around 1583 - 1586 cm^{-1} is assigned to the inner tube, and the G^+, at 1588 - 1611 cm^{-1} is attributed to the outer one. The outer tube is more sensitive to electrochemical charging as it is more exposed, and it exhibits a more pronounced shift of the G-band, revealing a higher charge carrier concentration at the outer tube.

The evidence of the presence of DWCNTs can also be observed analyzing the RBM. The frequencies of the RBM of the DWCNTs are unaffected by changing the potential. However, their intensities are modified with the applied potential, differently for inner and outer tubes. The attenuation observed in the RBM bands intensity promoted by electrochemical charging are more pronounced for the outer tubes which have larger diameters (156 cm^{-1}) and softer for the inner ones (200, 215, 221 and 259 cm^{-1}). While the bleaching of the band at 156 cm^{-1}, which corresponds to outer tubes, is observed already at ± 0.3 V, the bleaching of the inner tubes is postponed.

Figure 4 shows the radial breathing mode region of the Raman spectra of the steam treated samples excited by the different laser lines: 1.96 (a), 2.33 (b) and 2.54 eV (c), respectively. The normalized intensity of the RBM bands is shown as a function of treatment time in Figures 4.a.2. (1.96 eV), 4.b.2. (2.33 eV), and 4.c.2. (2.54 eV). According to the Kataura plot, in Figure 4.a.1, the region marked in orange, from 133 to 171 cm^{-1}, is assigned to semiconducting CNTs being in resonance with the third optical transition energy, E_{33}^S, and corresponds to a diameter distribution of 1.17 - 1.47 nm (semiconducting nanotubes at 1.96 eV). The yellow region represents the tubes excited via the E_{11}^M electronic transition, and it comprises the strong bands at 191 cm^{-1} (d_t= 1.05 nm) and at 215 cm^{-1} (d_t= 0.94 nm), assigned to metallic nanotubes. The grey region represents the RBM intensities that come from the E_{22}^S electronic transition, and it contains the band at ca. 255 cm^{-1} (d_t= 0.80 nm), thus corresponding to semiconducting nanotubes. Figure 4.b.1 shows the Raman spectra measured with the 2.33 eV excitation energy. The bands in the orange region, 142-195 cm^{-1}, correspond to nanotubes of d_t= 1.16-1.38 nm and represent the tubes that belong to the E_{33}^S transition. A strong band, in the yellow region, corresponding to tubes excited via the metallic transition (E_{11}^M) appears at ca. 274 cm^{-1} (d_t= 0.75). Results for the 2.54 eV laser excitation energy are presented in Figure 4.c.1. The bands in the orange region at ca. 157 and 177 (d_t= 1.26 and 1.13 nm) are assigned to semiconducting nanotubes that are in resonance via the E_{33}^S transition. The RBM modes in the yellow region at ca. 225 cm^{-1} (d_t= 0.90) and in the grey region at ca. 300 cm^{-1} (d_t= 0.69 nm) are assigned to metallic and semiconducting CNTs, the former being in resonance with the E_{11}^M and the latter with the E_{22}^S transition.

For all the excitation energies, there are abrupt changes in the intensity of the bands assigned to the E_{33}^S transition, which correspond to semiconducting nanotubes with large diameters. Consequently, mainly nanotubes with large diameter that correspond to outer nanotubes seem to be affected by the probed treatments. To study how the steam treatment affect tubes of different diameter, in the bottom panel of Figure 4, the height of the most intense Raman band in each region is represented versus time of treatment. In the case of steam treatment (Figure 4.a.2., 4.b.2, and 4.c.2) the RBM bands with lower frequency, corresponding to nanotubes with larger diameter, change their intensity more remarkably.

Figure 5 shows the D-band and the G-band for the as-received and steam treated CNTs. The G-band spectra are typical for CNTs bundles where the widths of the G-band are about 20 cm^{-1} (isolated nanotubes display smaller widths) and are centered at 1588 cm^{-1}.[32] The broadening of the G-band indicates that semiconducting and metallic carbon nanotubes are in resonance at the used laser excitation energies. When nanotubes bundles are excited in resonance with the transition of metallic nanotubes, the G^- is broadened.[33]

As nanotubes with different diameters are in resonance at different laser energies, the as-received and treated samples were measured by Raman spectroscopy using 3 different energies: 1.96 eV (633 nm), 2.33 eV (532 nm) and 2.54 eV (488 nm) to examine the effect on different diameters. The D-band appears at 1347 cm^{-1} using 2.54 eV and 2.33 eV and at 1320 cm^{-1} using 1.96 eV as excitation energy, since the frequency of the D-band is laser energy dependence.[34] In order to evaluate the amount of defects in the samples, in Figure 6 we represent the intensity ratio

between D and G-bands (the A_D/A_G ratio), calculated from the integrated areas (A_D and A_G, respectively).

As observed in Figure 6, the A_D/A_G ratio decreases as the time of treatment increases. This correlation is consistent with the fact that amorphous carbon presented in the samples is removed within steam treatment.[31] Besides, studying the lowering tendency of the A_D/A_G ratio with the time of treatment, we can observe that no significant number of new defects were created.

In agreement with the Raman analysis, HRTEM inspection of the steam treated CNTs also reveals that the sidewall structure of the CNTs has been well preserved after the steam treatment (Figure 7a and b). Furthermore, since short CNTs with a low degree of structural defects are of interest for the growth and shielding of one-dimensional compounds, we filled a sample of CNTs treated with steam for 25 h with NaI. The metal halide was encapsulated by molten phase high temperature filling, which results in the formation of filled closed-ended CNTs.[35] Having closed or corked ends allows the removal of the external material (using an appropriate solvent) whilst preserving the encapsulated compounds.[35-36] Therefore, being NaI water soluble, the NaI crystals external to the CNTs were removed by stirring the sample in water. Figure 7c shows a Z-contrast HAADF STEM image of the resulting sample where filled carbon nanotubes can be clearly seen. In this imaging modality NaI appears with a brighter contrast (white strings in the image) than carbon from the nanotubes (pale grey in the image). This confirms the ability of the steam treated CNTs to seal materials in their interior. If the CNTs had structural defects, release of the encapsulated NaI would have occurred during the washing protocol employed for the removal of the external NaI.

Apart form filled CNTs, some small bright dots are also visible in Figure 7c that correspond to residual inorganic particles, still present after the steam and HCl purification. The amount of inorganic material present in a sample of CNTs can be easily determined by thermogravimetric analysis, where the residue obtained after the complete combustion of the carbonaceous species corresponds to the inorganic material in its oxidized form. TGA in air was performed for all the samples and the inorganic residues are summarized in Figure 8 (See SI for the TGA curves, Figure S3). It is worth noting that the onset of the combustion temperature shifts to higher temperatures when increasing the steam treatment, in agreement with the lower content of defects determined by Raman analysis of the samples. EDX analysis of the inorganic solid residue obtained after the complete combustion of the as- received material, reveals the presence of iron and silicon (SI, Figure S4). Whereas iron is used for the growth of the nanotubes, and its presence in the elemental form has been previsouly determined by X-ray photoelectron spectroscopy anaylsis,[14b] silicon is more likely to be present as silica in agreement with the large oxygen peak visible in the EDX spectrum. The amount of iron and silica in the samples cannot be discerned from the TGA data. Therefore, the contribution from the metal impurities (iron) was calculated from magnetic measurements using a superconducting quantum interference device (SQUID) magnetometer[37] and is also included in Figure 8. The amount of Fe in the as-received CNTs is 1.4 wt.% (SQUID). This amount of Fe is converted to Fe_2O_3 during the TGA under flowing air. Thus, 1.4 wt.% of iron will result in a 2.0 wt.% of Fe_2O_3 residue after the complete combustion of the sample. The amount of silica can be determined from the difference between the inorganic solid residue of the as-received material (4.6 wt.% by TGA) and the amount of iron oxide (2.0 wt.%) that is obtained by oxidation of the iron present in the sample during the TGA. Thus, the as-received CNTs contain 2.6 wt.%. of silica. As it can be seen in the figure, the amount of iron nanoparticles are greatly decreased after treating the as-received CNTs with steam for 4 h followed by an HCl wash down to 0.4 wt.% Fe (SQUID). The decrease in the metal content is also reflected as a decrease in the TGA residue. During the steam purification the graphitic shells coating the catalytic metal particles are removed.[14b] Consequently, the exposed catalytic particles can be easily dissolved by treatment with hydrochloric acid and account for the decrease observed in the iron content. The metal particles still present after prolonged steam treatments and HCl wash are likely to be buried inside very thick graphitic particles, which are not completely removed during the steam oxidation. This leads to a relative increase in the iron content when increasing the time of steam treatment. The increase is batch dependent and reflects the thickness of the graphitic shells that stealth the Fe nanoparticles. In the present case, it only raises from 0.4 wt.% after 4 h steam to 0.7 wt.% after 25 h (SQUID), but larger increases have been reported.[14b] Since neither steam nor HCl are able to remove silica from the sample, the continuous combustion of carbon upon increasing the steam treatment time results in a continuous relative increase in the amount of silica in the samples, reflected as an increase in the amount of inorganic solid residue determined by TGA.

Conclusions

We have investigated the role that the time of steam treatment plays on both the length distribution and the structure of single-walled and double-walled CNTs. Raman spectroscopy and *in situ* Raman spectroelectrochemistry with 3 different excitation energies (1.96 eV (633 nm), 2.33 eV (532 nm) and 2.54 eV (488 nm) prove that wider and outer nanotubes are the ones where more significant changes in the RBM intensities are observed upon the steam treatment, especially in the case of prolonged treatments (25 h). The inner tubes are protected by the outer ones; hence they are less affected by the treatment. The steam treated samples present a continuous decrease in the A_D/A_G ratio, being an indication of the removal of the more defective nanotubes and amorphous carbon. A different trend is observed on the length distribution of the CNTs. Short nanotubes (ca. 200 nm median length) are already achieved after 10 h of steam. The length distribution of the samples obtained after 10 h, 15 h and 25 h of steam treatment does not present significant differences, as assessed by non-parametric statistical tests. We have shown that individual nanotubes can be imaged by means of SEM by employing ortho-dichlorobenzene as a dispersing agent, thus allowing a fast assessment of the length distribution. The low degree of structural defects in the steam shortened CNTs allows the containment of selected payloads in their interior (NaI in the present study). We envisage the use of such short high-quality CNTs in areas such as advanced electronics, memory storage and in the biomedical field.

Experimental Section

Material

Chemical vapor deposition (CVD) grown Elicarb® carbon nanotubes were provided by Thomas Swan & Co. Ltd. The as-received powder "Elicarb® SWNT" contains a mixture of both single-walled and double-walled carbon nanotubes (according to the supplier). Since this will be a subject of investigation in the present study, we will refer to this material as carbon nanotubes (CNTs).

Methods

As-received CNTs (400 mg) were finely ground with an agate mortar and pestle and spread inside a silica tube (4 cm in diameter) which served as a sample holder. The silica tube was then placed inside an alumina tube (5 cm in diameter) in the center of a tubular furnace. Steam was introduced at a rate of 0.58 mL/min by purging a continuous flow of argon (Carburos Metálicos, 99.999 % purity) through hot water (98 °C). The system was initially purged with Ar for 2 h to ensure the complete removal or air. Then, the furnace was annealed at a rate of 300 °C/min and dwelled at 900 °C for selected periods of time: 4 h, 10 h, 15 h and 25 h. According to previous reports, steam removes the amorphous carbon and graphitic shells that sheathe catalytic metal particles employed for the growth of the CNTs.[14] Therefore, each of the steam treated samples was independently refluxed with 6 M HCl to dissolve the exposed metal particles. The sample was collected by filtration onto polycarbonate membrane (0.2 µm pore size, Whatman® Nucleopore) and rinsed with distilled water until the pH of the filtrate was neutral. The collected solid powder was dried overnight at 100 °C and used for further characterization.

Prolonged steam treated CNTs (25 h + HCl) were filled with sodium iodide (Sigma Aldrich, 99.999 % purity) by molten filling. Both materials were ground together in a weight ratio 1:10 (CNTs:NaI) inside an argon filled glove box until the mixture presented a uniform color. The sample was placed inside a silica tube and sealed under vacuum before annealing it at 900 °C for 12 h. In order to remove the excess of NaI, external to the CNTs, the collected sample was dispersed in distilled water and stirred for 3 h at 60 °C. After this period of time filled tubes (NaI@CNTs) were recovered by filtration onto a polycarbonate membrane. The sample was dried overnight at 100 °C.

Equipment and characterization

Thermogravimetric analysis (TGA) of the samples was performed in a NETZSCH-STA 449 F1 Jupiter instrument. Samples were analyzed under flowing air at a heating rate of 10 °C/min until 900 °C. Magnetic measurements were done in a Superconducting Quantum Interference Device (SQUID) magnetometer (LOT-Quantum Design Iberia). A diamagnetic gelatin capsule was filled with 5-7 mg of sample. Data was acquired with an applied field from -15.000 Oe to +15.000 Oe at 10 K to obtain the hysteresis loops. The sample holder contribution was subtracted in all the measurements. The amount of iron in each of the analyzed samples was determined by taking into account the magnetic saturation of the bulk material (Ms_{Fe} = 221.7 emu·g^{-1}). Raman spectra were acquired using a LabRAM HR Raman spectrometer (Horiba Jobin-Yvon), and laser excitation energies of 2.54 and 2.33 eV (488 and 532 nm, respectively, Ar/Kr laser, Coherent) and of 1.96 eV (633 nm, He-Ne). A 50x objective was used with a laser spot of about 1 µm. The laser power was 1 mW and the spectral resolution was

1 cm^{-1}. Each sample was measured in multiple regions. Raman mapping was conducted with lateral steps of 1 µm (both in *X* and *Y* directions) on rectangular areas with varying sizes (49 data points or 900 data points for each map). The samples were measured under ambient conditions. The Raman spectroelectrochemistry was performed in a 3 electrode cell assembled in a glove box. The measured CNTs were cast on a Pt wire from their dispersion in methanol, which was employed as the working electrode. Another Pt wire was employed as a counter electrode and an Ag wire as a reference electrode. An Autolab PGSTAT (Ecochemie) potentiostat was used to apply potential. The electrolyte solution was $LiClO_4$ (0.2 M) dissolved in dry acetonitrile. The potential was ramped to ± 1.5 V in steps of 0.3 V, and Raman spectra were acquired at constant potential at every step. The high frequency component of the G^- band, the G^+, was fitted by a Lorentzian line shape, whereas the low frequency component, the G^-, was fitted using a Breit-Wigner-Fano (BWF) lineshape. The D-band was fitted by a Lorentzian lineshape. The length distribution of the samples was determined from analysis of SEM images using Digital Micrograph software. The sample for SEM observation was prepared as follows: first, a tiny amount of nanotubes was sonicated in 3 mL of ortho-dichlorobenzene (Sigma Aldrich, 99 %) between 30 to 45 min in order to achieve a good dispersion (the suspension presented a homogenous grey color). Then, about ten drops of this dispersion were placed onto a copper grid coated with a carbon film, and left to dry. SEM studies were carried out on a FEI Magellan 400L XHR using the In-Lens Detector (TLD) at a landing energy of 2 kV achieved by beam deceleration mode. In these conditions, surface sensitive images with spatial resolution below 1 nm are obtained, allowing the visualization of individual single- and double-walled carbon nanotubes. Three hundred isolated nanotubes were measured to determine the length distribution of as-received and treated CNTs. The sample of NaI@CNTs was dispersed in ethanol, and few drops were deposited on copper grids. Energy dispersive X-ray spectra were acquired at 20 kV on a FEI Quanta 200 FEG ESEM coupled to an Oxford Instruments EDX detection system. TEM images were acquired with a FEI Tecnai G2 F20 at 200 kV and scanning transmission electron microscopy images (STEM) on a FEI Magellan 400L XHR SEM operated at 20 kV with a high angle annular dark field (HAADF) detector.

Acknowledgements

The research leading to these results has received funding from the People Programme (Marie Curie Actions) of the European Union's Seventh Framework Programme FP7/2007-2013/ under REA grant agreement n° 290023 (RADDEL). ICN2 acknowledges support from the Severo Ochoa Program (MINECO, Grant SEV-2013-0295), and M. Kalbac the support from MSMT project LL1301. The authors are grateful to Thomas Swan & Co. Ltd. for providing Elicarb® SWNT. M. Kierkowicz and E. Pach are enrolled in the PhD Program in Materials Science at UAB.

Keywords: shortening • cutting • Raman spectroscopy • Raman spectroelectrochemistry • scanning electron microscopy

[1] M. F. L. De Volder, S. H. Tawfick, R. H. Baughman and A. J. Hart, *Science* **2013**, *339*, 535-539.
[2] Y. Liu, Y. Zhao, B. Sun and C. Chen, *Acc. Chem. Res.* **2013**, *46*, 702-713.
[3] a) K. Pulskamp, S. Diabaté and H. F. Krug, *Toxicol. Lett.* **2007**, *168*, 58-74; b) H. Ali-Boucetta, A. Nunes, R. Sainz, M. A. Herrero, B. Tian, M. Prato, A. Bianco and K. Kostarelos, *Angew. Chem., Int. Ed.* **2013**, *52*, 2274-2278.
[4] M. Pumera, *Chem. Eur. J.* **2009**, *15*, 4970-4978.
[5] a) L. Meng, R. Chen, A. Jiang, L. Wang, P. Wang, C.-z. Li, R. Bai, Y. Zhao, H. Autrup and C. Chen, *Small* **2013**, *9*, 1786-1798; b) X. Liu, L. Guo, D. Morris, A. B. Kane and R. H. Hurt, *Carbon* **2008**, *46*, 489-500; c) R. Hamilton, Z. Wu, S. Mitra, P. Shaw and A. Holian, *Part. Fibre. Toxicol.* **2013**, *10*, 57.
[6] a) Y. Wang, J. Zhang, J. Zang, E. Ge and H. Huang, *Corr. Sci.* **2011**, *53*, 3764-3770; b) M. Q. Tran, C. Tridech, A. Alfrey, A. Bismarck and M. S. P. Shaffer, *Carbon* **2007**, *45*, 2341-2350.
[7] a) N. Rubio, C. Fabbro, M. A. Herrero, A. De La Hoz, M. Meneghetti, J. L. G. Fierro, M. Prato and E. Vázquez, *Small* **2011**, *7*, 665-674; b) C. Zapata-Massot and N. Le Bolay, *Chem. Eng. Process.* **2008**, *47*, 1350-1356.
[8] S. R. B. Lustig, E. D.; French, R. H.; Gierke, T. D.; Harmer, M. A.; Hietpas, P. B.; Jagota, A.; McLean, R. S.; Mitchell, G. P.; Onoa, G. B.; Sams, K. D., *Nano Lett.* **2003**, *3*, 1007-1012.
[9] S.-H. Jeong, O.-J. Lee, K.-H. Lee, S. H. Oh and C.-G. Park, *Chem. Mater.* **2002**, *14*, 1859-1862.
[10] F. Banhart, J. Li and M. Terrones, *Small* **2005**, *1*, 953-956.
[11] a) J. Liu, A. G. Rinzler, H. J. Dai, J. H. Hafner, R. K. Bradley, P. J. Boul, A. Lu, T. Iverson, K. Shelimov, C. B. Huffman, F. Rodriguez-Macias, Y. S. Shon, T. R. Lee, D. T. Colbert and R. E. Smalley, *Science* **1998**, *280*, 1253-1256; b) J. Y. Li and Y. F. Zhang, *Appl. Surf. Sci.* **2006**, *252*, 2944-2948; c) M. V. Shuba, A. G. Paddubskaya, P. P. Kuzhir, S. A. Maksimenko, V. K. Ksenevich, G. Niaura, D. Seliuta, I. Kasalynas and G. Valusis, *Nanotechnology* **2012**, *23*, 495714; d) C.-C. Lin, B. T. T. Chu, G. Tobias, S. Sahakalkan, S. Roth, M. L. H. Green and S.-Y. Chen, *Nanotechnology* **2009**, *20*, 105703.
[12] K. Flavin, I. Kopf, E. Del Canto, C. Navio, C. Bittencourt and S. Giordani, *J. Mater. Chem.* **2011**, *21*, 17881-17887.
[13] a) X. Chen, H. Chen, C. Tripisciano, A. Jedrzejewska, M. H. Rümmeli, R. Klingeler, R. J. Kalenczuk, P. K. Chu and E. Borowiak-Palen, *Chem. Eur. J.* **2011**, *17*, 4454-4459; b) L. Cabana, B. Ballesteros, E. Batista, C. Magén, R. Arenal, J. Oró-Solé, R. Rurali and G. Tobias, *Adv. Mater.* **2014**, *26*, 2016-2021; c) K. G. Ujjal, M. F. J. C. Pedro, B. Yoshio, F. Xiaosheng, L. Liang, I. Masataka and G. Dmitri, *Sci. Tech. Adv. Mater.* **2010**, *11*, 054501; d) X. Liu, I. Marangon, G. Melinte, C. Wilhelm, C. Ménard-Moyon, B. P. Pichon, O. Ersen, K. Aubertin, W. Baaziz, C. Pham-Huu, S. Bégin-Colin, A. Bianco, F. Gazeau and D. Bégin, *ACS Nano* **2014**, *8*, 11290-11304; e) M. Martincic and G.

Tobias, *Expert Opin. Drug Deliv.*, **2015**, 12, 563-581; f) M. V. Bracamonte , M. Melchionna, A. Stopin, A. Giulani, C. Tavagnacco, Y. Garcia, P. Fornasiero , D. Bonifazi and M. Prato, *Chem. Eur. J.* **2015**, *21*, 12769-12777.
[14] a) G. Tobias, L. Shao, C. G. Salzmann, Y. Huh and M. L. H. Green, *J. Phys. Chem. B* **2006**, *110*, 22318-22322; b) B. Ballesteros, G. Tobias, L. Shao, E. Pellicer, J. Nogués, E. Mendoza and M. L. H. Green, *Small* **2008**, *4*, 1501-1506.
[15] L. Cabana, X. Ke, D. Kepić, J. Oro-Solé, E. Tobías-Rossell, G. Van Tendeloo and G. Tobias, *Carbon* **2015**, *93*, 1059–1067.
[16] a) T. C. Reich S., Maultzsch J., *Carbon Nanotubes: Basic Concepts and Physical Properties*, John Wiley & Sons, **2004**, p; b) R. S. A. Jorio; M. S. D., G. Dresselhaus, *Raman Spectroscopy in Graphene Related Systems*, John Wiley & Sons, **2011**, p.
[17] P. P. B. C. Araujo P. T., Dresselhaus M.S., Sato K., Saito R., Jorio A., *Phys. E* **2010**, *42*, 1251–1261.
[18] D. G. Dresselhaus M. S., Saito R., Jorio A., *Physiscs Reports* **2005**, *409*, 47-99.
[19] a) N. Bendiab, L. Spina, A. Zahab, P. Poncharal, C. Marliere, C. Marlière, J. L. Bantignies, E. Anglaret and J. L. Sauvajol, *Phys. Rev. B* **2001**, *63*; b) P. W. Chiu, G. S. Duesberg, U. Dettlaff-Weglikowska and S. Roth, *Appl. Phys. Lett.* **2002**, *80*, 3811-3813.
[20] W. Zhou, J. Vavro, F. Borondics, N. M. Nemes, J. E. Fischer, K. Kamarás and D. B. Tanner, *Phys. Rev. B* **2005**, *71*.
[21] M. Kalbac and L. Kavan, *J. Phys. Chem. C* **2009**, *113*, 16408-16413.
[22] a) L. Kavan, P. Rapta, L. Dunsch, M. J. Bronikowski, P. Willis and R. E. Smalley, *J. Phys. Chem. B* **2001**, *105*, 10764-10771; b) L. Kavan and L. Dunsch in *Electrochemistry of Carbon Nanotubes*, *Vol. 111* Eds.: A. Jorio, G. Dresselhaus and M. Dresselhaus), Springer Berlin Heidelberg, **2008**, pp. 567-604.
[23] a) Z. Chen, R. Hauge and R. Smalley, *J. Nanosci. Nanotechnol.* **2006**, *6*, 1935-1938; b) S. Wang, Z. Liang, B. Wang and C. Zhang, *Nanotechnology* **2006**, *17*, 634.
[24] X. X. Wang, J. N. Wang, H. Chang and Y. F. Zhang, *Adv. Funct. Mater.* **2007**, *17*, 3613-3618.
[25] P. Liu and T. Wang, *Appl. Phys. A* **2009**, *97*, 771-775.
[26] a) X. Fu, J. Wang, J. Ding, H. Wu, Y. Dong and Y. Fu, *Compos. Sci. Technol.* **2013**, *87*, 170-173; b) A. Yaya, C. P. Ewels, P. Wagner, I. Suarez-Martinez, A. Gebramariam Tekley and L. Rosgaard Jensen, *Eur. Phys. J. A* **2011**, *54*.
[27] J. L. Bahr, E. T. Mickelson, M. J. Bronikowski, R. E. Smalley and J. M. Tour, *Chem. Comm.* **2001**, 193-194.
[28] a) D. Tasis, N. Tagmatarchis, V. Georgakilas and M. Prato, *Chem. Eur. J.* **2003**, *9*, 4000-4008; b) A. Battigelli, C. Ménard-Moyon, T. Da Ros, M. Prato and A. Bianco, *Adv. Drug Deliv. Rev.* **2013**, *65*, 1899-1920; c) E. Del Canto, K. Flavin, D. Movia, C. Navio, C. Bittencourt and S. Giordani, *Chem. Mat.* **2011**, *23*, 67-74; d) C. Ménard-Moyon, C. Fabbro, M. Prato and A. Bianco, *Chem. Eur. J.* **2011**, *17*, 3222-3227; e) V. Georgakilas, A. Kouloumpis, D. Gournis, A. Bourlinos, C. Trapalis and R. Zboril, *Chem. Eur. J.* **2013**, *19*, 12884-12891.
[29] S. G. King, L. McCafferty, V. Stolojan and S. R. P. Silva, *Carbon* **2015**, *84*, 130-137.
[30] A. Jorio, R. Saito, M. Hunter, J. H. Hafner, C. M. Lieber, T. McClure, G. Dresselhaus and M. S. Dresselhaus, *Phys. Rev. Lett.* **2001**, *86*, 1118-1121.
[31] L. Kavan, M. Kalbáč, M. Zukalová, M. Krause and L. Dunsch, *Phys. Chem. Chem. Phys.* **2004**, *5*, 274-277.
[32] A. Jorio, A. G. Souza, G. Dresselhaus, A. G. Souza-Filho, M. S. Dresselhaus, A. K. Swan, M. S. Ünlü, B. B. Goldberg, M. A. Pimenta, J. H. Hafner, C. M. Lieber and R. Saito, *Phys. Rev. B* **2002**, *65*.
[33] M. A. Pimenta, A. Marucci, S. A. Empedocles, M. G. Bawendi and E. B. Hanlon, *Phys. Rev. B* **1998**, *58*, 16016-16019.
[34] A. Marucci, P. Corio, S. D. M. Brown, M. A. Pimenta, E. B. Hanlon, S. A. Empedocles, M. G. Bawendi, G. Dresselhaus and M. S. Dresselhaus, *Braz. J. Phys.* **2000**, *30*, 423-427.
[35] L. Shao, G. Tobias, Y. Huh and M. L. H. Green, *Carbon* **2006**, *44*, 2855-2858.
[36] a) L. Shao, T.-W. Lin, G. Tobias and M. L. H. Green, *Chem. Comm.* **2008**, 2164-2166; b) P. Luksirikul, B. Ballesteros, G. Tobias, M. G. Moloney and M. L. H. Green, *Carbon* **2010**, *48*, 1912-1917; c) G. Tobias, B. Ballesteros and M. L. H. Green, *physica status solidi (c)* **2010**, *7*, 2739-2742.
[37] a) T. Kolodiazhnyi and M. Pumera, *Small* **2008**, *4*, 1476-1484; b) B. Pacakova-Bittova, M. Kalbac, S. Kubickova, A. Mantlikova, S. Mangold and J. Vejpravova, *Phys. Chem. Chem. Phys.* **2013**, *16*, 5992-6000.

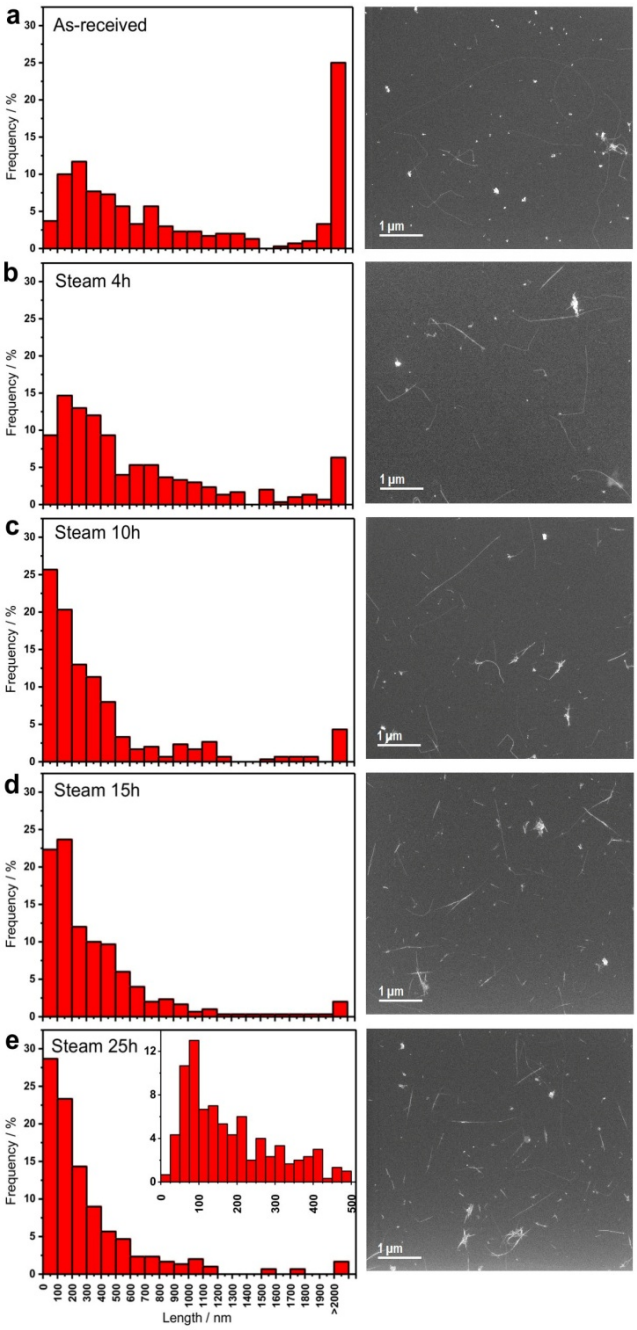

Figure 1. Analysis of the length distribution of as-received and steam treated CNTs for different periods of time. a) as-received, b) 4 h, c) 10 h, d) 15 h and e) 25 h steam treated CNTs (after an HCl wash). Histograms are presented on the left panel and representative SEM images on the right panel of the figure.

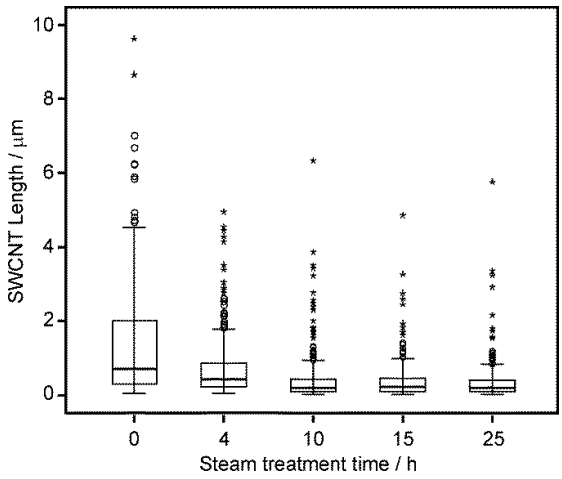

Figure 2. Box plot analysis of the as-received CNTs (0 h) and steam-treated CNTs for 4 h, 10 h, 15 h and 25 h (after an HCl wash). Empty circles indicate outliers and asterisks far outliers. The lower and maximum adjacent observations are represented with horizontal lines at the end of the whiskers.

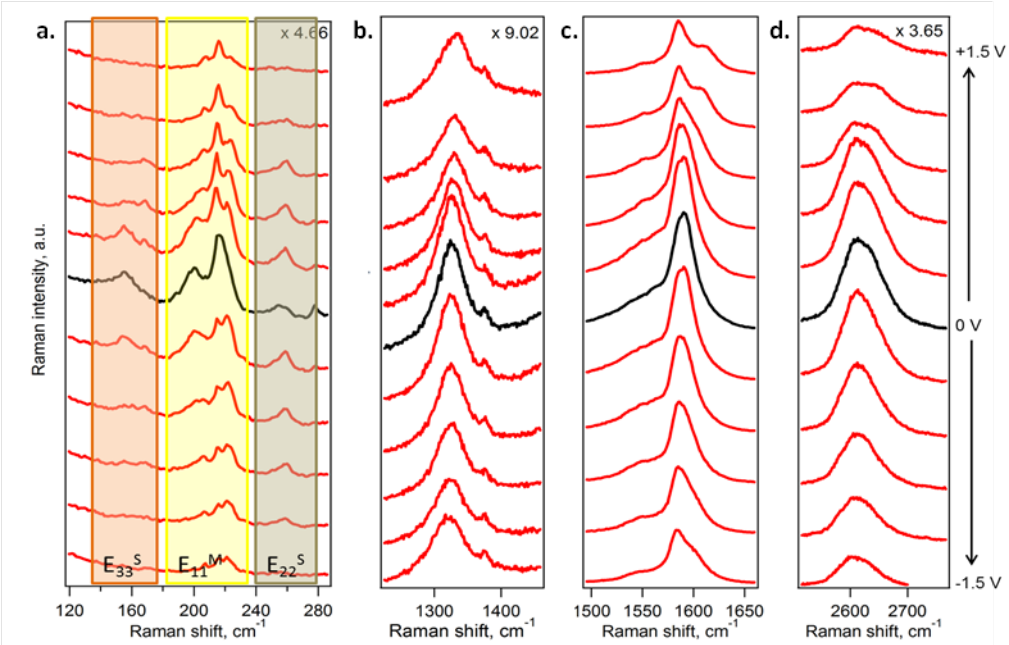

Figure 3. Raman spectra of the as-received CNTs at different potentials in the spectral regions of a. RBM, b. D-band, c. G-band, and d. G'-band. The electrode potential range is from -1.5 to 1.5 V vs Ag/Ag^+ (from bottom to top). The spectra in black correspond to the 0 V potential. The electrochemical potential change between the curves in the figure is 0.3 V. The spectra were acquired using 1.96 eV laser excitation energy. The spectra are offset for clarity

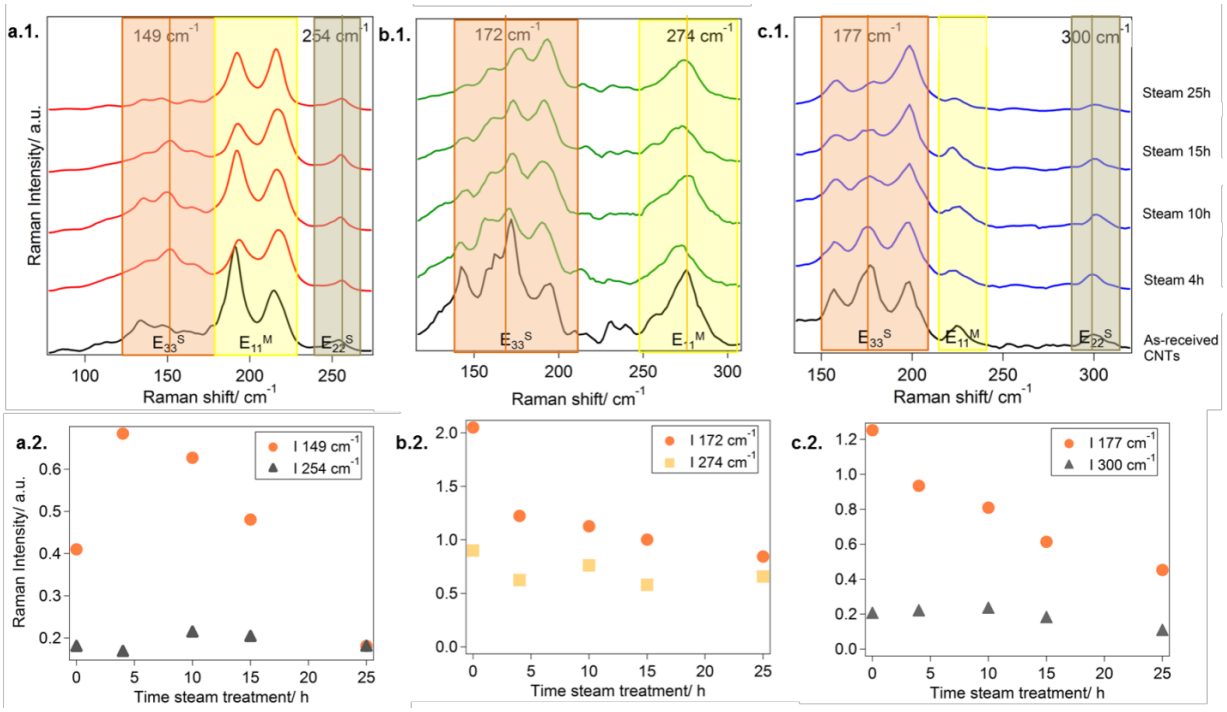

Figure 4. Resonance Raman spectra (RBM region) of pristine CNTs (black line) and steam treated CNTs for different periods of time (HCl washed), excited by different laser lines a. 1.96 eV (633 nm), b. 2.33 eV (532 nm) and c. 2.54 eV (488 nm). In figures a.1, b.1. and c.1., the orange, yellow and grey regions correspond to the E_{33}^{S}, E_{11}^{M} and E_{22}^{S} electronic transitions, respectively. Each spectrum is an average based on 900 (1.96 eV) and 49 spectra (2.33 and 2.54 eV) measured in different points. a.2., b.2. and c.2. show the normalized Raman Intensity of the RBM modes versus time of steam treatment for excitation energies of 1.96 eV, 2.33 eV and 2.54 eV, respectively. Spectra in a.1. and intensities in a.2. were normalized by the RBM band at 215 cm^{-1}. Spectra in b.1. and intensities in b.2. were normalized by the RBM band at 195 cm^{-1}, Spectra in c.1. and intensities in c.2. were normalized by the RBM band at 199 cm^{-1}. The spectra are offset for clarity.

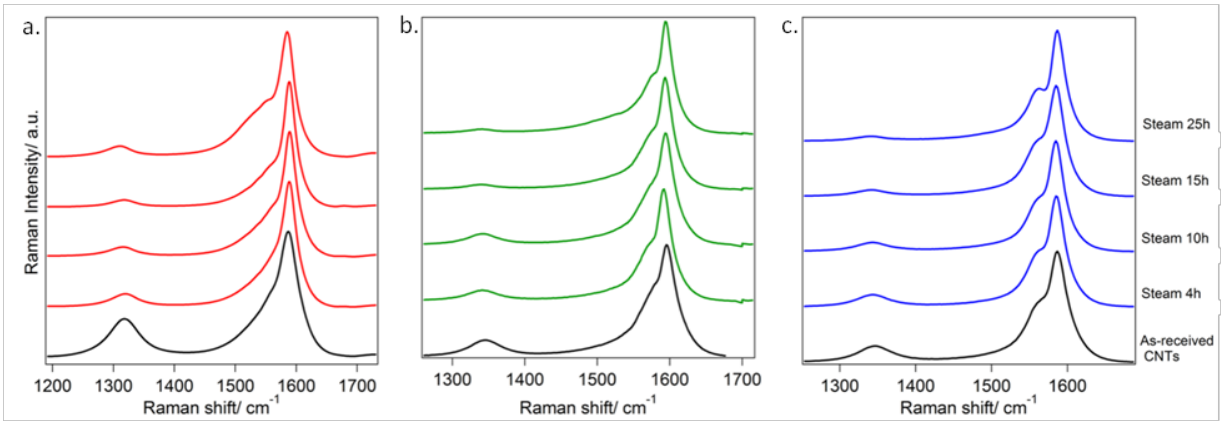

Figure 5. Resonance Raman spectra (D and G-band region) of pristine CNTs (black line) and steam treated CNTs for different periods of time (HCl washed), excited by different laser lines a. 1.96 eV (633 nm), b. 2.33 eV (532 nm) and c. 2.54 eV (488 nm). Each spectrum is an average based on 900 (1.96 eV) and 49 spectra (2.33 and 2.54 eV) measured in different points. The spectra are offset for clarity.

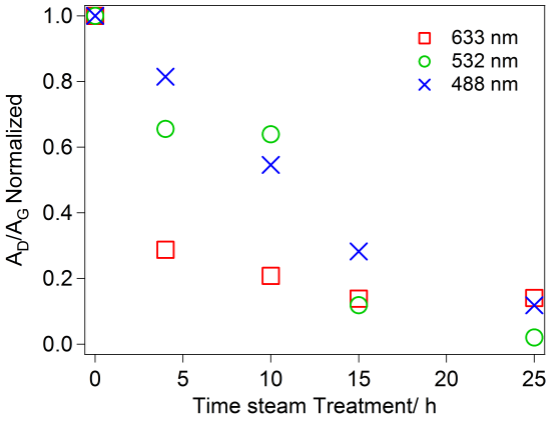

Figure 6. A_D/A_G ratio of the as-received CNTs (0 h treatment) and steam treated CNTs (HCl washed) for different periods of time. The samples were excited using 1.96 eV (red squares), 2.33 eV (green circles) and 2.54 eV (blue crosses) laser energies

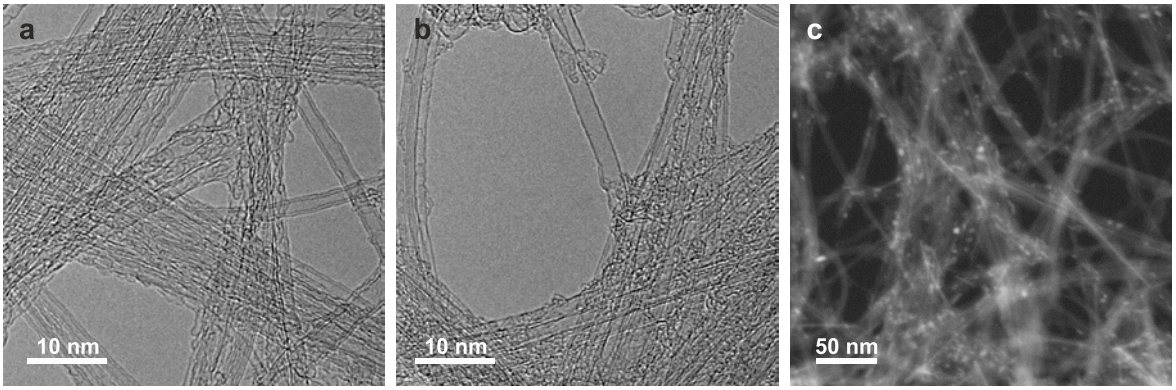

Figure 7. Electron microscopy analysis of steam treated samples. a) HRTEM of as-received CNTs, b) 25 h of steam treated CNTs (after an HCl wash), and c) HAADF STEM image of NaI filled CNTs

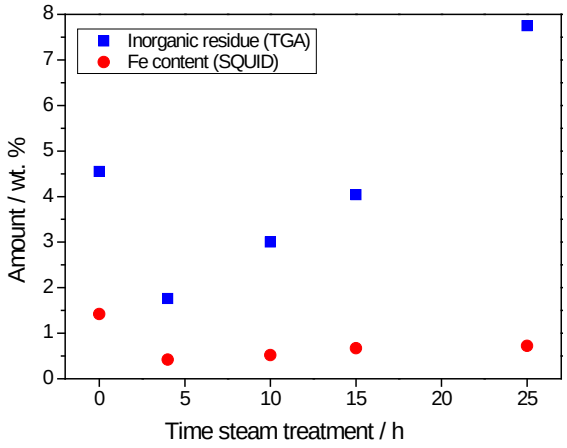

Figure 8. Amount of iron (determined by SQUID) and inorganic solid residue (determined by TGA) in the as-received (0 h) and steam treated samples during 4 h, 10 h, 15 h and 25 h (after an HCl wash)

Table 1. Descriptive analysis of the length distribution for as-received CNTs and steam-treated CNTs during 4 h, 10 h, 15 h and 25h (after an HCl wash). Note that the lower observation is the same than the lower adjacent observation. See Figure 2 for the corresponding box plot analysis.

Sample	N Number of measured CNTs	Median (nm)	Lower adjacent observation (nm)	Q1 25^{th} percentile (nm)	Q3 75^{th} percentile (nm)	Maximum adjacent observation (nm)	Maximum observation (nm)
As-received	300	711	41	297	2009	4517	9621
4 h	300	420	33	215	845	1783	4943
10 h	300	198	15	84	423	932	6320
15 h	300	223	6	101	455	985	4857
25 h	300	191	23	92	388	831	5756